Journal of Power Sources 570 (2023) 233058

Contents lists available at ScienceDirect

Journal of Power Sources

journal homepage: www.elsevier.com/locate/jpowsour

Predicting the cost of a 24 V soluble lead flow battery optimised for PV applications

Diarmid Roberts [a], Ewan J. Fraser [b], Andrew Cruden [b], Richard G. Wills [b], Solomon Brown [a,*]

[a] University of Sheffield, UK
[b] University of Southampton, UK

HIGHLIGHTS

- Optimisation of a 24 V soluble lead flow battery for use in PV powered charging hub.
- Definition of reference system, and use to test cost and performance sensitivity.
- Methane sulphonic acid, then bipolar plates were largest cost components presently.
- Deposits of at least 0.5 mm are critical for low cost (<£100/kWh) 4h system.
- Cost of DC system (excluding assembly) could fall below £50/kWh.

ABSTRACT

Providing reliable electricity from small-scale renewable power is an important challenge for emerging economies. The soluble lead flow battery (SLFB) is a promising battery for this application, as it has a simple architecture making it relatively robust, and a lifetime of 2000 cycles demonstrated at the cell level. Also, the electrolyte is manufacturable directly from spent lead acid batteries. There is a need for techno-economic models to allow the cost/performance of a complete system to be defined and optimised.

Such a model is defined here for the first time and used in a multi-objective optimisation to design a 24 V system for a charging hub in Sierra Leone. A 4 h duration was found to be optimal, and electrolyte for a 3.5 kW/14 kWh system would fit in a 1000 L IBC.

Methanesulfonic acid was found to be the largest cost component of the 4 h system, with graphitic bipolar plates next. Both have low raw material costs, and in an optimistic scenario a total component cost of <£50/kWh would be achieved, half that of current NMC Li-ion cells. The greatest technical risk to achieving low cost is deposit thickness of lead dioxide. This important research gap should be addressed.

1. Introduction

The need for energy storage to enable a high penetration of variable renewable power generation in grid infrastructures is well known [1]. Redox flow batteries (RFBs) are one subset of energy storage technologies in which energy is stored and released by flowing redox active species in solution through an electrochemical reactor. The key benefits of RFBs vary according to the chemistry, but include long lifetime (vanadium RFB (VFB) in particular), low redox species cost (most types, particularly iron) and high recyclability (most types).

The soluble lead flow battery (SLFB) is a type of RFB in which solid lead and lead dioxide are deposited at the negative and positive electrodes during charge and then dissolved back into the electrolyte as Pb^{2+} ions during discharge. Unlike the conventional lead acid battery (LAB), the Pb^{2+} ions are highly soluble in the aqueous electrolyte, which is based on methanesulfonic acid (MSA) rather than sulphuric acid. The following redox equations describe this process:

$$Negative\ electrode: \quad 2e^- + Pb_2 + \rightleftharpoons Pb \quad E_0 = -0.13\ V\ vs.\ SHE \tag{1}$$

$$Positive\ electrode: \ Pb_2 + +2H_2O \rightleftharpoons PbO_2 + 4H^+ + 2e^- \quad E_0 = +1.46\ V\ vs.\ SHE \tag{2}$$

$$Cell: \quad 2Pb^{2+} + H_2O \rightleftharpoons PbO_2 + Pb + 4H^+ \quad E_0 cell = 1.59\ V \tag{3}$$

A number of benefits have been claimed for the SLFB when compared to other RFB systems. As there is only one electrolyte, the balance of plant costs (pumps, valves, piping) should be cheaper than both vanadium flow batteries (VFB) and zinc-bromine flow batteries (ZFB), and in the flow-by, flat-electrode configuration there is no need for a separator [2]. It has also been shown that the electrolyte can be manufactured

* Corresponding author.
E-mail address: s.f.brown@sheffield.ac.uk (S. Brown).

https://doi.org/10.1016/j.jpowsour.2023.233058
Received 7 December 2022; Received in revised form 1 March 2023; Accepted 4 April 2023
Available online 12 April 2023

from spent lead acid batteries using a simple process [3,4]. Lastly, the less chemically aggressive nature and biodegradability of the MSA used in the electrolyte compared to other acids used in RFBs has been claimed as an advantage from an environmental perspective [5,6].

A weakness of the SLFB system is low energy density, at 20–40 Wh/L for the electrolyte, although the impact of this will depend on the supply chain and the location in which the SLFB will be deployed. Another weakness is the difficulty of obtaining good quality lead dioxide deposits that dissolve readily to support discharge. This aspect of the SLFB has attracted the greatest share of the research effort, and a system that achieves 2000 cycles has been demonstrated by Verde *at al.* in a simple beaker cell [7]. This lifetime, being greatly superior to that achievable by the LAB forms the main technical motivation for development of the SLFB over that technology, the other being the greater achievable depth of discharge [3]. However, the lifetime demonstrated by Verde et al. was achieved using a specific charge-discharge duty cycle; there is no research describing the performance of a SLFB under a fluctuating charge/discharge profile, as would be required in a micro-grid application.

Several models have been published on the physical performance of the SLFB. Shah et al. defined a two dimensional model of a single cell SLFB, which described both the electrochemistry and mass transport phenomena [8]. Given the importance of deposit uniformity on the electrodes, Nandanwar and Kumar developed a one dimensional model to study this problem [9]. The model correctly predicted that deposition is more readily achieved at the upstream end of the electrodes, which during discharge leads to active area reduction from the downstream end. Fraser, Ranga Dinesh and Wills reported a model for electrolyte conductivity, and validated it experimentally [10]. The primary conductivity phenomenon is the increase with state of charge as protons are liberated via the oxidation of Pb^{2+} (equation (2)). Nandanwar et al. modelled a novel pump-less SLFB at the single cell level, where the electrolyte flow is driven by convection due to the change in electrolyte density as Pb^{2+} is added or removed from solution [11].

Unlike for other RFB, there is an important gap in the SLFB literature regarding engineering and techno-economic models. In such models, some resolution is sacrificed (e.g. mass transport modelling) in order to run quickly enough to perform multiple iterations to optimise aspects of the system design [12]. These models may also incorporate pumping losses and shunt currents at the stack level, making them more relevant to commercial systems [13]. Although the SLFB can achieve a round-trip efficiency of almost 80% at the single cell level [7] (comparable with VFB and pumped hydro storage), there is no detailed experimental literature on pilot scale multi-cell stacks [2], such as that published for the VFB [14]. Hence the degree to which pumping and shunt currents will decrease the system efficiency is an important knowledge gap.

Furthermore, no detailed techno-economic analysis has been published to the best of the authors' knowledge. In a 2018 review, Krishna et al. cite a report that predicts costs of £1075/kW and £80/kWh [2]. However, this report did not include a description of the methodology used, or provide a breakdown of the components and moreover is not available online. This gap in the SLFB literature is in contrast to that of the VFB, where models of varying detail have been employed to measure and optimise both the cost of the system [15] and its economic benefit [16–18].

Given the absence of engineering models and techno-economic analysis of commercially relevant SLFB systems, this article makes a number of important novel contributions to the field.

- A performance model for a 24 V system has been developed within a load following algorithm, so that the performance of the SLFB may be simulated in micro-grid type applications.
- A multi-objective optimisation approach has been used to determine a suitable system for a PV based micro-grid case study, by varying the electrolyte volume and the length and width of the electrodes.
- By using this model and present cost estimates, a reference undivided flow-by SLFB system has been defined at 2–4 kW scale with 4 h duration for approximately optimal CAPEX vs. load met in a PV powered micro-grid.
- The critical cost components of this SLFB have been identified.
- A sensitivity study on performance assumptions has been performed, showing which technical parameters are critical, and where future research should focus.

2. Methods

2.1. The case study

In this case study, the SLFB serves as an energy store for a portable battery charging hub deployed by Mobile Power [19]. Two weeks of power consumption data from an installation in Sierra Leone were used in the simulations reported here. The peak power consumption of the hub would be 2 kW if all slots were filled and active, although this does not happen often due to use patterns. Example days are shown in Fig. 1.

The hub and SLFB are powered from a 5 kWp PV array, the output of which was simulated using the PVGIS model for a location close to the deployment [20]. The timestep used in the simulation was 15 min, the resolution of the power consumption data, hence the hourly resolution PV data were interpolated.

2.2. Multi-objective optimisation (MOO)

In this section, the method employed to determine the optimal power and energy capacity of the SLFB for the case study mentioned above is described. A problem in energy storage sizing is that the cost of the system requirements increases super-linearly with the desired fraction of demand met [21]. This is due to variability in the availability of renewable power from day to day. For this reason, it is not necessarily economical to meet all of the existing demand. A multi-objective optimisation for minimization of cost and maximisation of fraction of demand met was therefore performed. The optimal specification was then obtained manually from the "knee point" where the gradient of utility versus cost levels off, indicating diminishing returns. The genetic algorithm NSGA II [22] was applied using the PYMOO package for Python [23]. An overview of the process is given in Fig. 2.

During the optimisation, the design variables were bounded as shown in Table 1. The upper bound on l_{BPP}, the bipolar plate length relates to the size of the IBC vessel, so that the stack could be shipped inside it. The bipolar plate width, w_{BPP} bounds were set to avoid

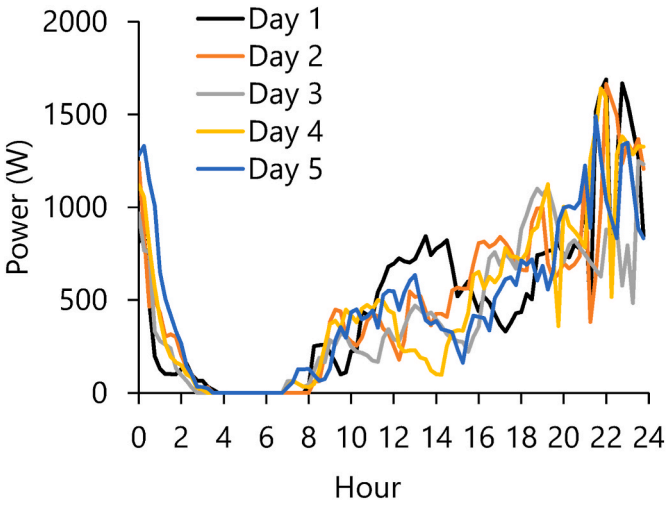

Fig. 1. Example power consumption data for the portable battery pack charging hub in Sierra Leone.

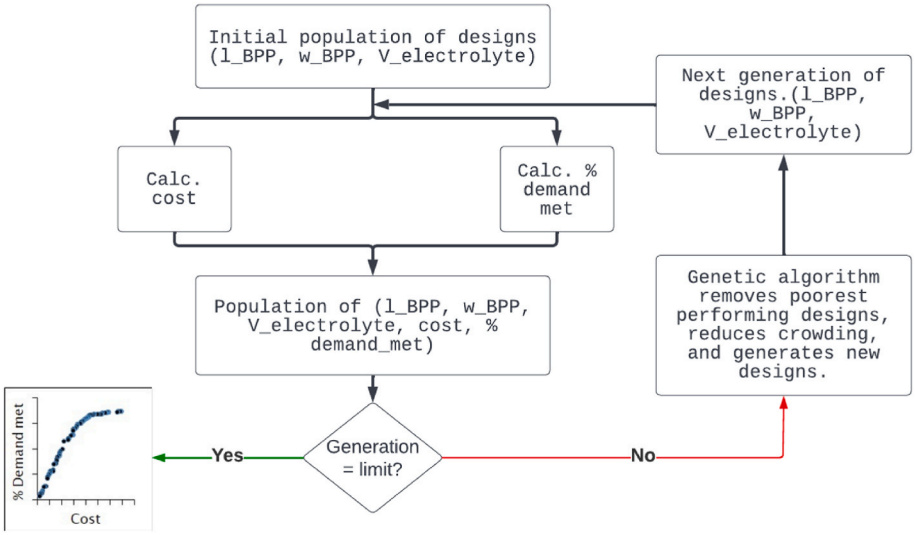

Fig. 2. Multi-objective design optimisation process for SLFB component sizing based on the genetic algorithm NSGAII.

Table 1
SLFB design variables for the first optimisation and their respective bounds. l_{BPP} and l_{BPP} are the length and width of the bipolar plates respectively, and $V_{Electrolyte}$ is the volume of electrolyte.

Symbol	Description	Bounds
l_{BPP}	Length of bipolar plate electrodes	0.4 m–0.9 m
w_{BPP}	Width of bipolar plate electrodes	0.1 m–0.25 m
$V_{Electrolyte}$	Volume of electrolyte	0.25 m^3–0.70 m^3

excessive aspect ratios. The bounds on volume were set based on pre-calculations regarding the daily duty load profile.

In both cases the optimisation was subject to a constraint on the lead oxide deposit thickness on the cathode, defined by:

$$\frac{V_{Electrol.} C_{Pb} (\overline{SOC} - \underline{SOC}) M_{PbO2}}{w_{BPP} l_{BPP} n_{series} n_{stacks} \sigma_{PbO2}} \leq \overline{\delta_{PbO2}} \quad (4)$$

Where, in addition to the parameters defined in Table 2, M_{PbO2} and σ_{PbO2} are respectively the molar mass (kg/mol) and density (kg/m^3) of lead (IV) oxide.

2.3. Utility objective

The utility objective was the fraction of the charging hub demand that can be met from the PV and the SLFB in the studied period. This was determined using the greedy algorithm shown in Fig. S1. The determination of the shunt currents involves solving a system of equations (see 2.3.1) based on Kirchoff's law, and this is the slowest part of the simulation. For this reason, the algorithm first attempts to match the power surplus/deficit by ignoring shunt currents and iterating on the external current density $i_{ext.}$ (parts 1 and 2 in Fig. S1).[1] An iterative adjustment is then made by subtracting the simulated shunt current density [24] from the external current density to give the internal current density $i_{int.}$. As this is lower than the external current density, during charging the overpotential is lower as a result, and the external current density is incremented to compensate in for this reduction in power uptake. During discharge, the shunt currents lead to a greater voltage drop, hence the current is decremented (i.e. made more negative).

An initial value for $i_{ext.}$ (A./m^2) at time t is obtained by:

Table 2
parameters defining the performance of the SLFB in the load following algorithm used to simulate utility.

Symbol	Description	Units	Value (base scenario)	Source
n_{Series}	Number of series cells in stack	–	16	For 24 V nominal stack.
n_{Stacks}	Number of stacks in the system	–	1	
$\bar{i}_{Chg.}$	Max. charge current density	mA/cm^2	50	[25]
$\bar{i}_{Dischg.}$	Max. discharge current density	mA/cm^2	−50	[25]
OCV	Open cell voltage	V	1.78	[3]
c_{Pb}	Concentration of $Pb(MSA)_2$ in discharged fresh electrolyte	M	0.7	[3]
c_{MSA}	Concentration of MSA in electrolyte	M	1	[3]
$\underline{SOC}$	Minimum permitted SOC	–	0	[3]
$\overline{SOC}$	Maximum permitted SOC	–	0.7	[3]
$\overline{\delta_{PbO2}}$	Maximum permitted lead oxide deposit thickness	m	0.001	[2]
ρ_{PbO2}	Resistivity of lead dioxide	Ωm	1×10^{-5}	
ρ_{Pb}	Resistivity of lead	Ωm	2.2×10^{-7}	
ρ_{BPP}	Resistivity of bipolar plate	Ωm	3×10^{-4}	Brochure
δ_{BPP}	Thickness of bipolar plate	m	6×10^{-4}	Brochure
δ_{Cell}	Cell gap	m	0.01	Typical
$\eta_{chg.}$	Scalar approximation of kinetic overpotential during charge	V	0.23	Typical
$\eta_{dischg.}$	Scalar approximation of kinetic overpotential during discharge	V	0.11	Typical
$\underline{v}$	Minimum flow velocity through cell	m/s	0.02	[26–28]
h_{pump}	Pump head	m	2	Estimate
ε_{pump}	Pump efficiency	–	0.4	[29]
Δ_{SOC}	Maximum permitted relative difference in SOC across cell	–	0.2	[13]
P	Maximum electrolyte density	kg/m^3	1220	[30]
$s_{electrolyte}$	Electrolyte conductivity as function of free ions.	S/m	SOC dependent	[10]

[1] This nominal quantity is defined as the apparent current at the terminals divided by the electrode area.

$$i_{ext.,t} = \frac{P_{PV,t} - P_{load,t} - P_{pump}}{OCV w_{BPP} l_{BPP} n_{series} n_{stacks}} \quad (5)$$

with terms defined in Table 3, and where $P_{PV,t}$ is the power available from the PV array, $P_{load,t}$ is the power demand of the charging hub P_{pump} the pumping power is defined by:

$$P_{pump} = \frac{P g h_{pump} \overline{Q}}{\varepsilon_{pump}} \quad (6)$$

where the maximum electrolyte flow rate $\overline{Q}$ (m^3/s) is defined by:

$$\overline{Q} = \max\left(Q_{Stoich.}, Q_{Vel.}\right) \quad (7)$$

where $Q_{Stoich.}$ is the maximum stoichiometric flow rate, defined by:

$$Q_{Stoich.} = \frac{w_{BPP} l_{BPP} n_{series} n_{stacks} \overline{i}_{Chg.}}{c_{Pb}(1 - \overline{SOC}) F \Delta_{SOC}} \quad (8)$$

which stipulates that the maximum charge current density be supportable at the highest SOC while restricting the relative change in SOC across the cell to be greater than the threshold value Δ_{SOC}. The flow rate required to achieve the minimum cell flow velocity, $Q_{Vel.}$, is defined by:

$$Q_{Vel.} = \underline{v} \delta_{cell} w_{BPP} n_{series} n_{stacks} \quad (9)$$

It should be noted that in the majority of SLFB designs described in this work, the velocity condition was limiting. The working cell voltage during charging is calculated first by:

$$V_{cell} = OCV + i_{ext.} ASR + \eta_{chg.} \quad (9)$$

And later, in the shunt current adjustment step by substituting $i_{ext.}$ with $i_{int.}$ For discharge, the faradaic overpotential, $\eta_{dischg.}$ is subtracted. The area specific resistance ($\Omega.m^2$) is calculated by:

$$ASR = \delta_{Pb}\rho_{Pb} + \delta_{PbO2}\rho_{PbO2} + \delta_{BPP}\rho_{BPP} + \frac{\delta_{cell}}{s_{electrolyte}} \quad (10)$$

where, in addition to the terms defined in Table 2, δ_{Pb} and δ_{PbO2} are the average lead and lead dioxide deposit thicknesses, calculated from the fresh electrolyte lead concentration, the state of charge, and the density of lead and lead dioxide.

The stack power is calculated by:

$$P_{stack} = i_{ext.} w_{BPP} l_{BPP} n_{series} n_{stacks} v_{cell} \quad (11)$$

Once the algorithm converges, the resultant state of charge is calculated by:

$$SOC_t = SOC_{t-1} + \frac{i_{int.} w_{BPP} l_{BPP} n_{series} n_{stacks} \tau}{C} \quad (12)$$

Table 3
dimensions of SLFB components that define the flow path.

Symbol	Description	Value base scenario (m)
$l^{Pipe}_{P\to M}$	Pump- > manifold pipe length	2
$D^{Pipe}_{P\to M}$	Pump- > manifold pipe ID	0.027
D_M	Manifold ID	0.045
$l^{Pipe}_{M\to C}$	Manifold- > cell pipe length	0.02
$D^{Pipe}_{M\to C}$	Manifold- > cell pipe ID	0.0064
l_{Inlet}	Inlet length[a]	0.05
$D^{Throttle}_{Inlet}$	Inlet flow restriction diameter	0.0025
$l^{Throttle}_{Inlet}$	Inlet flow restriction length	0.02
l_{Outlet}	Outlet length[a]	0.05
$D^{Throttle}_{Outlet}$	Outlet flow restriction diameter	0.0025
$l^{Throttle}_{Outlet}$	Outlet flow restriction length	0.04
l^{M}_{Outlet}	Outlet manifold depth	0.01

[a] The thickness of the inlet and outlet sections is the same as the cell gap, which is a variable (see Table 2).

where C is the coulombic capacity (Ah) of the fresh electrolyte, a function of electrolyte volume and lead concentration and τ the timestep of the simulation (h). After the algorithm is run across all periods, the % demand met objective is calculated by:

$$\%_{demand_{met}} = \sum_{t \in P_{PV} - P_{load} < 0} \frac{P_{stack,t} + P_{pump}}{P_{PV,t} - P_{load,t}} \quad (12)$$

where the denominator represents the total net load (exc. Storage) in the period, and the numerator the load satisfied by the SLFB (recalling that $P_{stack,t}$ is negative when discharging).

The operational efficiency of the SLFB may then be calculated over a period starting and ending with the same SOC by:

$$Eff. = \frac{-\sum_{t \in P_{stack,t} < 0} P_{stack,t} - P_{pump}}{\sum_{t \in P_{stack,t} > 0} P_{stack,t} + P_{pump}} \quad (12)$$

with the denominator giving the total input and the numerator the total output.

The utility model was parametrized using the values given in Table 2.

2.3.1. Shunt current modelling

When RFB cells are stacked in bipolar configuration, such that the cells are in series electrically but the electrolyte flows in parallel through each, shunt currents occur. These cause continual discharge as electrons pass across the BPP, balanced by current flowing in the electrolyte through the manifold. The first consequence of shunt currents is reduced coulombic efficiency. Additionally, in a hybrid RFB like the SLFB, as the electric current through the bipolar plate is higher in the center of the stack, the deposition there will lag behind that at the outer plates [31]. During discharge, the stripping of deposits will be faster in the center of the stack. Overall, there will still be deposits on the outer plates when the inner plates become bare and the stack voltage drops. Over time this will lead to progressive build-up on the outer plates, necessitating maintenance intervention. In this work, the background discharge from each BPP due to shunt currents was estimated using the equivalent circuit model reported for a stack of single compartment cells by Kaminski et al. [24]. The channel and manifold resistances required for this model were calculated by summing the resistances of the individual geometric components in Table 3.

The impact on SOC was modelled by averaging the shunt current and subtracting it from the external current. Possible improvements to this modelling approach are discussed in the conclusions.

It was assumed that when the system is idle, the pump stops, the electrolyte drains from the stack and there is no conductive path for shunt currents.

To model shunt currents (and pumping requirements) a basic SLFB stack configuration was defined with a combination of rectangular and circular cross sections. Schematics of the manifold/stack and a single cell are shown in Fig. 3.

The measurements of each feature highlighted in Fig. 3 are given in Table 3. These are fixed throughout the study.

2.3.2. Pumping requirements

Previous studies on the optimal design of RFBs have included a calculation of the pumping power as the product of flow rate and outlet pressure over the pump efficiency [13]. Although this approach allows a value to be placed on efficient flow field design, it assumes that there are no constraints on pump design. From inspection of specification sheets for centrifugal pump families it was found that the rated outlet pressure increases with the rated flow rate [29]. Staying close to the rated pressure and flow rate is desirable for long pump life as well as high efficiency. It was assumed that a number of small pumps with a rated head of 2 m will be used to achieve the target flowrate [32]. The pumping power was therefore a function of this pressure and the modelled flow

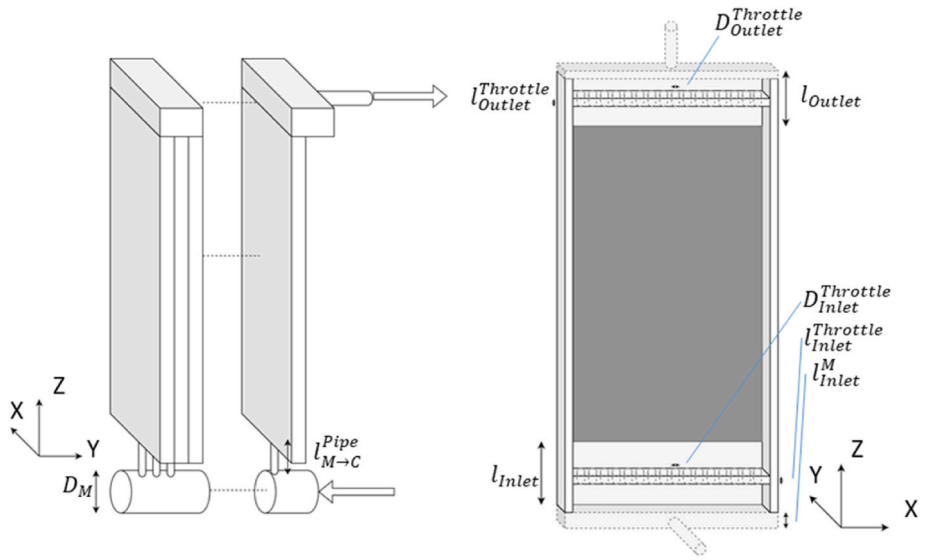

Fig. 3. Left: schematic of SLFB stack showing inlet and outlet manifold. Right: schematic of cell unit showing inlet and outlet flow restrictions and electrode. Neither figure to scale.

rate. The pump efficiency was assumed to be 40%, which appears realistic at the rated pressure [29], although an efficiency of 60% has been assumed elsewhere [13]. Further investigation will be required to understand whether upgrades are required to resist the MSA in the electrolyte for several years.

The flow requirement for the electrolyte was defined as the maximum of the flow velocity requirement and the stoichiometry requirement (see Eqn. (9)). The pump treatment was conservative in that the same flow was applied whenever the system was active, whereas in reality a variable power pump could be used.

2.4. Cost objective

In the MOO, the cost of the system attributable to the variable components (BPP, pumps and chemicals) was defined by:

$$C_{Var.} = C_{BPP} l_{BPP} w_{BPP} n_{Series} n_{Stacks} + C_{Pump} \overline{Q} + V_{Electrolyte}(c_{Pb} M_{Pb} C_{Pb} + (2c_{Pb} + c_{MSA}) M_{MSA} C_{MSA}) \quad (13)$$

The cost parameters used in the base and alternative scenarios are listed in Table 4.

2.5. Additional cost modelling

The stack is the most complex part of the SLFB, and is potentially costly to manufacture due to the number of components. In this section we analyse the impact on the stack frame manufacture cost (£/kW) of the following factors.

1 Cell size
2 Number of components per cell
3 Size of production run.

The aim for large volume manufacturing of the stack is to use injection moulding, which has high upfront costs associated with mould fabrication, but low per-part costs. An interactive prototyping quotation tool was used to evaluate the cost of moulding the cell unit shown in Fig. 3.

The initial stack design consisted of 16 cells connected in series to give a 24 V nominal stack voltage, each with a 0.40 × 0.15 m electrode area. This stack was modelled as being capable of 650 W discharge at the maximum 50 mA/cm^2 current density. There are potential benefits to having smaller stack modules, for example having multiple modules in the system so that some could be idled at lower charging power in order to avoid a low current density on any stack, as there are indications that this may give poor deposit quality [7]. A smaller stack may also be more rigid, and give a lower pressure force normal to the flow direction, both of which can make sealing easier.

At commercial production levels (1 MW cumulative capacity) the per-part cost starts to dominate, as shown by the levelling out of the stack cost in Fig. S2. The per-part costs are dominated (78%) by the labour and machine time costs rather than the cost of the polypropylene feedstock.

The first design revision was therefore to develop a cell architecture that may be constructed as one part rather than two. Although the individual parts are more expensive, a saving of 41% was achieved (£196/kW to £115/kW) by making half as many of them.

Using the same rationale of minimizing the part count, the second design revision was to increase the electrode size to 400 × 250 mm, such that the 16 cell module was capable of 1.1 kW rather than 650 W, leading to a further 30% reduction (£80/kW).

Lastly, a quote was obtained for the 1 piece 1 kW stack from a larger prototyping company, with a considerably lower price of £41/kW. For the following system cost analysis, it was assumed that the cell manufacture cost would be either £41/kW for a 1-piece cell, or £69/kW for a 2-piece cell (via cost ratio given above). It is anticipated that further cost reductions will be possible as the cell design has not been optimised for manufacture, or material reduction.

3. Results

3.1. Optimizing the SLFB component sizing

The SLFB component sizing optimisation process was applied to 2 weeks of data from Mobile Power's example hub in Sierra Leone. The Pareto front for the base cost scenario is shown in Fig. 4.

It may be observed in Fig. 4 that the cost of increasing the utility of the SLFB increases almost linearly up to around 90%. In this domain, increases to the SLFB capacity produce an increase to the fraction of demand met on the majority of days. Above this, increasing the capacity gives a smaller increase to utility, as the incremental storage is not required every day, but just to cover days 8 and 9 in Fig. 5, where the PV output is lower. It is important to note that deciding how much of the potential load should be served will be a case by case matter. In the pay-

Table 4
cost parameters used in modelling of the SLFB. For stack manufacture, it was assumed that a cumulative production of 1000 MW is achieved. Where a price range is indicated, the base case is emboldened. TPO: typical price online.

Class	Item	Price (low/ mid/ high)	Unit	Quant.	Source
Energy	IBC	100	£	1	TPO
	Lead (as breaker paste)	0.55/ 0.825/ 1.1	£/kg	Var.	2022 PbA battery scrap price range with 10% markup.
	Methanesulfonic acid	0.5//3	£/kg	Var.	Low: BASF spending "high double digit million" figure (taken as £75 m) to expand production from 30,000 to 50,000 Mt p.a., spread over 10 years production, plus H_2SO_4 and CH_4 feedstock costs [33,34]. High: TPO China and India.
Power	BPP	10//87	£/m^2	Var.	High estimate based on marketing materials showing <€100/ m^2. Low estimate is arbitrary distance from £1/ m^2 raw materials cost.
	Injection moulded cell units in PP.	41/69	£/kW	–	Quotation, high is for 2 piece cell, low is for 1 piece.
	Pump	1.02	£/LPM	Var.	Cost of purchasing multiple units of low head centrifugal pump rated for 48 LPM at 2 M head 32.

as-you-go power case study here, all demand is treated equally, hence there will be some point where adding further storage capacity makes no economic sense (and adding more PV capacity may be a better choice).

Fig. 4 also shows that the BPP area must be increased in line with the electrolyte volume in order to increase the SLFB capacity. In the displayed region, the length of the BPP is already at a maximum, and it is the width that must be increased to reach higher % load met. The high aspect ratio of the cell is driven by penalties associated with a wider cell, both in the increase in flow required to maintain the flow velocity, and the decrease in shunt current resistance. In principal, pump cost and pumping losses will be opposing drivers, as both elevation head and in-cell flow resistance will increase with BPP length. However, the pressure drop through the cell is expected to be minimal compared to that across the throttle features shown in Fig. 3.

The SLFB specified for 90% load met has BPP electrodes that are 0.89 m long and 0.16 m wide, and an electrolyte volume of 361 L. The predicted peak output of the SLFB during the studied period was 1.64 kW, and the average discharge capacity (when fully cycled) was 6.84 kWh. This equates to a duration of 4.2 h. The round trip efficiency, defined as energy input over energy output across the two-week period (start and end SOC both 0), including pumping requirements and shunt current losses was 59%.

The current density data in Fig. 5 show that the internal current density reaches the 50 mA/cm^2 bound during both charge and discharge. At maximum SOC, the lead dioxide deposit thickness is 0.9 mm, which is below the 1 mm bound defined by Equation (4) hence the system is power constrained rather than energy constrained.

The shunt currents are greater at the outlet manifold than the inlet manifold, as the design of the latter (which has not been optimised) presents a lower resistance in the electrolyte channel. The shunt currents increase with SOC, as the electrolyte conductivity increases with free H^+ concentration [10]. The average shunt current while active is 2.01 mA/cm^2, versus an average terminal current of 23.4 mA/cm^2, equating to 8.6% coulombic loss.

There is scope to improve the efficiency of the SLFB with a more intelligent control system. Fig. 5 shows that improving upon the greedy algorithm could improve charging efficiency, as on the 2nd and 3rd days a lower charging current could be used, saving on ohmic losses.

3.2. Sensitivity study on performance assumptions

There are a number of performance related parameters that can be expected to influence the SLFB performance, but which have a high degree of uncertainty at present. The impact of this uncertainty was tested by varying each parameter by +50%, −50% or both.

In the previous section, it was demonstrated that the optimal stack has a high aspect ratio in order to minimize the required flow rate and shunt currents (although pressure drop was not modelled). Enquiries regarding manufacturing of a long cell unit indicated that this shape may

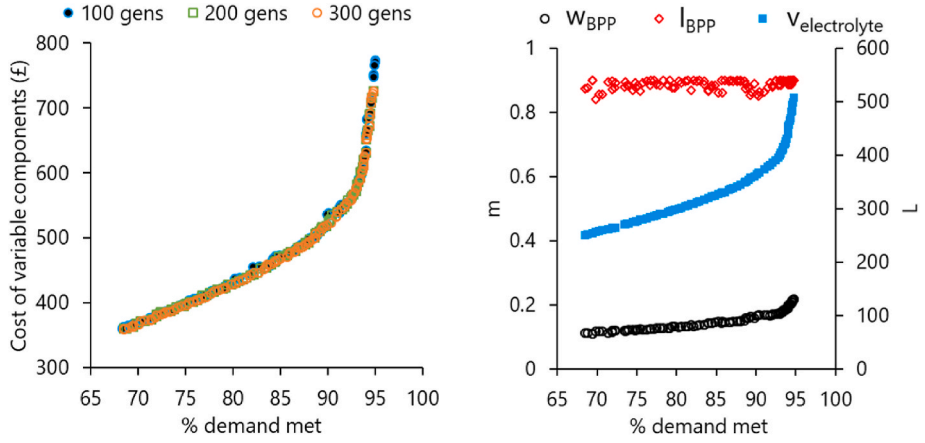

Fig. 4. Left: the Pareto front of cost versus utility for sizing of the SLFB bipolar plates and electrolyte volume to meet the power demand in the case study. Right: the variation in the optimal system design with utility (after 300 generations).

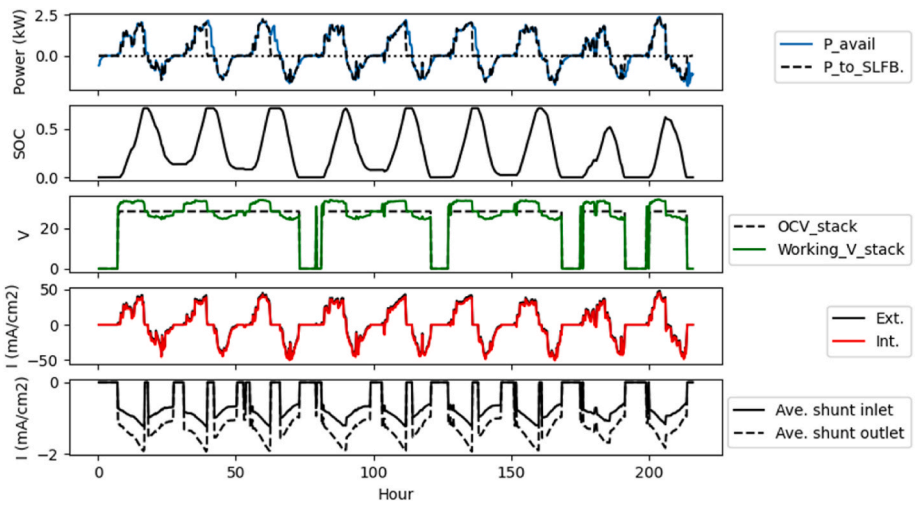

Fig. 5. The simulated operation of the SLFB shown for the first 9 days of the two week case study period.

be challenging, at least for subtractive machining and 3D printing, the techniques that are accessible for prototyping.

For this reason, cell designs based around a maximum BPP length of 0.40 m were investigated, with the number of stacks in the system being increased to 2 to compensate. The bounds on the other variables were tightened as described in Table 5 in order to focus on the knee point region in Fig. 4. The resultant Pareto fronts are shown in Fig. 6.

And solutions for each case are compared at a cost level of £550 in Table 6.

It is important to note the change of performance in the base case upon fixing the BPP length at 0.4 m. The simulated operational efficiency of the SLFB drops from 59% to 46.5% as a result of approximately doubling both the shunt currents and the pumping load along with the total flow cross section. Of these two sources of losses, shunt currents are much more important in the present design; reducing the shunt currents by 50% would increase the efficiency to 55.5% whereas reducing the required flow velocity (and hence pump specification) by the same degree only increases it to 47.7%.

Reducing the cell gap is attractive in principal because this would reduce the stack size (and hence component cost), reduce the cell resistance (most of which is due to the electrolyte), reduce the volumetric flow rate required to reach the target flow velocity and increase the shunt current resistance. However, the flow resistance will increase, and if the gap is too narrow there is an increased risk of electrical shorting and non-uniform flow, especially as the deposit thickness grows. Reducing the gap by 50% achieves a 50% flow reduction, with associated efficiency improvement, plus a small reduction in shunt currents, taking the efficiency to 49.4%.

Reducing the assumed maximum deposit thickness has a far stronger effect than increasing it, due to the reciprocal nature of the relationship with electrode area. In the 0.5 mm thickness case, the Pareto front was very short, and the cost was high. This was because the only feasible systems are at the upper bound of BPP width (0.30 m) and the lower bound of the electrolyte volume (<311 L). The efficiency of the system in this case was predicted to be only 37.8%, as shunt currents and pumping losses are very high.

Table 5
SLFB design variables and respective bounds for second stage optimisation where BPP length was fixed at 0.4 m and n_{Stacks} was increased to 2.

Symbol	Description	Bounds
w_{BPP}	Width of bipolar plate electrodes	0.1 m–0.3 m
$V_{Electrolyte}$	Volume of electrolyte	0.3 m^3–0.5 m^3

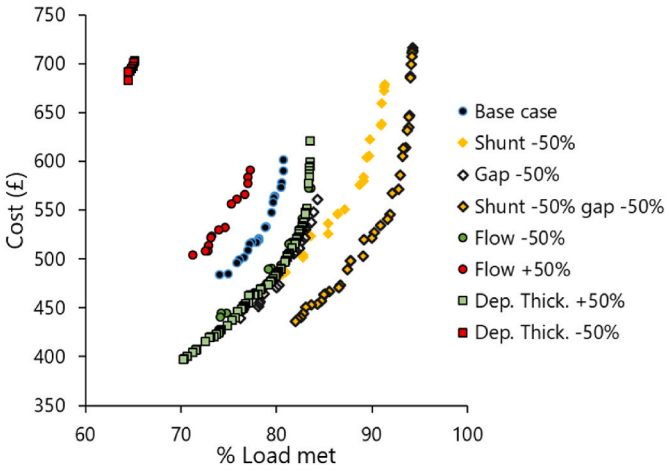

Fig. 6. Approximate Pareto fronts for minimal cost/maximum utility of SLFB. A number of performance assumptions are varied one by one from the Base case. In all cases the BPP length is fixed at 0.40 m and the number of stacks changed from 1 to 2.

3.3. Cost reduction scenarios

In addition to performance uncertainty, there is uncertainty relating to the costs of components. This is particularly the case for the BPP and MSA, which are both currently manufactured at small scale, but have very low raw material costs. For the former, roll-to-roll processing techniques have recently been introduced, which will allow far higher production volumes for a given equipment cost [35,36]. For MSA, a more efficient process has recently been reported [34] and is being scaled up by BASF [33].

Additionally, the cost reduction associated with designing a one-piece cell unit was tested, based on the data reported in the methods section.

Because the 6.1 kWh system in base case system in Table 6 only requires 354 L of electrolyte, the system would be undersized for the IBC vessel, adding to the £/kWh cost. A larger scale system was therefore tested, in which 5 stacks were specified rather than 2, and the electrolyte volume was multiplied by 2.5.

The impact of future component cost reductions on the SLFB system cost was tested in a combinatorial fashion with each of the performance cases in Table 6, and the results are shown in Fig. 7.

The boundary for costs was defined here to be comparable to cell

Table 6
Comparison of the predicted round trip efficiency, discharge capacity and % of load met that may be achieved for £550 under each performance assumption case. In all cases, l_{BPP} was fixed at 0.40 m *Under the reduced deposit thickness assumption, there was no SLFB that can be constructed for £550, so a £700 solution was included to illustrate the low efficiency and utility that results.

Scenario	w_{BPP} (m)	$V_{Electrol.}$ (L)	% Load met	Eff. (%)	Peak P_{out} (kW)	E_{out} (kWh)	E/P
Base	0.17	354	80	46.5	1.49	6.1	4.1
Max deposit thickness −50%*	0.30	310	65	37.8	1.85	5.0	2.7
Max deposit thickness + 50%	0.15	411	83	46.9	1.24	6.6	5.3
Min. flow vel. −50%	0.19	376	83	47.7	1.64	6.5	4.0
Min. flow vel. +50%	0.17	335	75	44.7	1.41	5.7	4.0
Shunt currents - 50%	0.17	356	87	55.5	1.57	6.5	4.1
Cell gap – 50%	0.19	377	84	49.4	1.59	6.4	4.0
Shunt currents −50%/Cell gap −50%	0.18	376	92	59.3	1.76	7.2	4.1

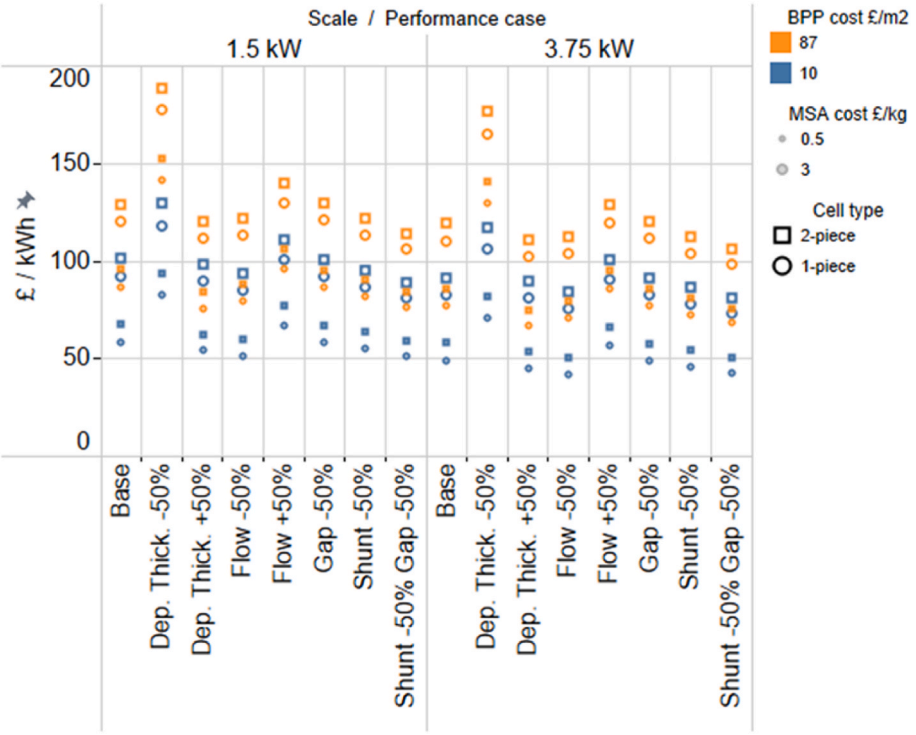

Fig. 7. the sensitivity of predicted costs for the SLFB system components (including stack frame manufacture) under various performance and design assumptions. Details of each design can be found in Tables 2 and 6.

costs for Li-ion batteries, i.e. all the components for producing DC power are included, but control was not. Manufacture was also not included, except for the stack frame moulding, which was treated as a purchased component.

The data in Fig. 7 show that reductions in the BPP cost have a great impact on system cost, and in most cases achieving a BPP cost of £10/m^2 would bring the system cost below £100/kWh. The cost of MSA was found to be a similarly important factor,

The greatest technical risk to the upfront system cost is restriction of the electrode deposit thickness, particularly at higher assumed BPP costs. If only 0.5 mm lead dioxide thickness were practical, it would be difficult to reach a cost below £100/kWh. Even if it were possible due to economies of scale in BPP and MSA manufacturing, there would still be problems with efficiency as shown in Table 6. The 1 mm base case thickness for lead dioxide was chosen as this was close to the 1 mm lead deposit target highlighted in a recent review [2].[2] A deposit thickness of 0.57 mm is implied in experimental work reported by Collins et al., but this was achieved in a 2 cm × 2 cm cell, and only 10 cycles were performed [37]. Verde et al. reported stable SLFB performance and excellent energy efficiency across 2000 cycles [7], and Jaiswal et al. recently reported 500 cycles [25], but in both cases this was for a 1h charge at 20 mA/cm^2, which corresponds to a lead dioxide thickness of only 0.1 mm.

Increasing the scale of the unit from ~1.5 kW to ~3.75 kW reduces the cost of the IBC from £16/kWh to £7/kWh. For the rightmost scenario in Fig. 7, the breakdown of component costs is shown in Fig. 8 alongside the base case.

Fig. 8 shows that based on present cost estimates, MSA was predicted to be the largest cost component of a 4h SLFB, with BPP the second largest. There is scope for the component costs of the SLFB to fall far below the current material costs of NMC Li-Ion cells, which have actually risen since 2020. However, the manufacturing costs for the Li-ion cells only increase the total to £113/kWh due to the scale and automation of the process. Estimating the manufacturing cost of the SLFB is out with the scope of this article, however Ha and Gallacher estimated in 2015 that the "unit price less materials" of a VFB would be lower than that of Li-ion cells at 2 GW annual production scale [35]. Also, in that

[2] The constraint of 1 mm max PbO_2 used herein is slightly more conservative as PbO_2 is less dense than Pb. It corresponds to 0.83 mm.

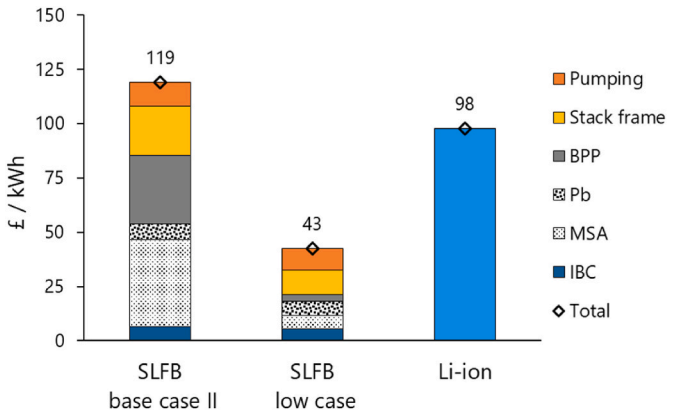

Fig. 8. Left: comparison of materials costs for a 3.75 kW SLFB under base (2-piece cell) and low cost scenario (1-piece cell, low settings for BPP and MSA cost, shunt −50% and gap −50%) with a 2022 estimate of LIB materials cost [38].

analysis, the manufacturing cost included several components (BPP, stack frame) which are already included in the above analysis. The simpler flow path and cell structure of the SLFB should in principle lead to cheaper manufacture than for the VFB.

4. Conclusions

In this work the specification of an SLFB for a PV microgrid was optimised against both a cost and utility objective. In the base scenario, a 1.64 kW 4h duration system was found to give the best utility before diminishing returns began. The optimal cell configuration was found to have a high aspect ratio (0.16 m wide by 0.9 m long BPP electrode, where 0.9 m was the upper bound). The simulated efficiency of this system was 59%, despite the flow path not being optimised for shunt current reduction, and a conservative assumption that the pump always operated at the same flow rate.

Due to anticipated issues with manufacturing long components, a system with 2 stacks and a fixed electrode length of 0.4 m was next defined. The present cost of components (including stack frame manufacture) is estimated at £98-£120/kWh (excluding control and assembly) assuming that a deposit thickness of 1 mm may be reliably achieved. Methanesulfonic acid was predicted to be the largest cost component of a 4h duration SLFB, followed by the graphitic bipolar plates. Both of these components have the potential for future price decreases as more efficient manufacturing techniques have recently been introduced, and the raw material costs are minimal. With reductions in MSA and BPP costs, this range could fall as low as £43-£56/kWh, making the SLFB cheaper at the DC level than NMC Li-ion cells.

The greatest risk to the system cost is an inability to reliably deposit lead and lead oxide at the assumed thickness of 1 mm, with thinner deposits increasing component cost and reducing efficiency. As testing of deposits of this thickness has not been performed across many cycles, there is an important gap in the knowledge of the SLFB which future research must address.

In the present work, the simulated shunt currents in each cell were averaged so that an average efficiency and change in SOC could be simulated. Improving the model to simulate the differing deposit thickness across the cells in the stack would be useful, as it would give a prediction of how often a strip cycle must be performed. There is also the potential for uneven deposition due to concentration gradients through the cell which would lead to premature voltage drop on discharge. Although Nandanwar and Kumar have developed a model for this process [9], including it within the optimisation model would have led to impractical run times. The constraint in Equation (8) was included in order to scale the electrolyte flow so that the gradient in lead concentration would never be greater than 20%. This allowed the cost of mitigating uneven deposits to be estimated. However, further modelling and experimental work is required to validate this approach.

Given the predicted higher efficiency of a high aspect ratio cell, more work is required to understand the manufacturability of such a component, especially via injection moulding. Although a common planar cell architecture has been studied in this work, the model could be readily adapted to optimise the design of novel cylindrical architectures which have recently been modelled and demonstrated for hybrid flow batteries [9,39].

Lastly, although the SLFB has potential to undercut the costs of other battery technologies, the efficiency is lower (although further reductions in the shunt current are expected to increase this further). A levelised cost study is therefore required to factor in the increased charging cost. Such a study should also cover the expected lifetime of the SLFB, although this is also dependent on further testing at relevant deposit thicknesses.

CRediT authorship contribution statement

Diarmid Roberts: Conceptualization, Methodology, Formal analysis, Writing – original draft, Writing – review & editing, Visualization. **Ewan J. Fraser:** Writing – original draft, Writing – review & editing, Visualization. **Andrew Cruden:** Writing – review & editing, Funding acquisition. **Richard G. Wills:** Writing – review & editing, Funding acquisition. **Solomon Brown:** Methodology, Writing – review & editing, Funding acquisition.

Declaration of competing interest

The authors declare that they have no known competing financial interests or personal relationships that could have appeared to influence the work reported in this paper.

Data availability

The authors do not have permission to share data.

Acknowledgements

The authors would like to thank UK Aid from the UK Government through the Faraday Institution and the Transforming Energy Access Program (Grant number FIEE-002 – Reclaimed Electrolyte, Low Cost Flow Battery RELCo-Bat); however, the views expressed do not necessarily reflect the UK government's official policies. They would also like to thank project partner Mobile Power for providing data from a deployment of their MOPO charging hub product.

Appendix A. Supplementary data

Supplementary data to this article can be found online at https://doi.org/10.1016/j.jpowsour.2023.233058.

References

[1] M. Sterner, I. Stadler, Handbook of Energy Storage, Springer, 2019, https://doi.org/10.1007/978-3-662-55504-0.
[2] M. Krishna, E.J. Fraser, R.G.A. Wills, F.C. Walsh, Developments in soluble lead flow batteries and remaining challenges: an illustrated review, J. Energy Storage 15 (2018) 69–90, https://doi.org/10.1016/j.est.2017.10.020.
[3] K. Orapeleng, R.G.A. Wills, A. Cruden, Developing electrolyte for a soluble lead redox flow battery by reprocessing spent lead acid battery electrodes, Batteries 3 (2) (2017) 1–13, https://doi.org/10.3390/batteries3020015.
[4] K. Orapeleng, R.G.A. Wills, A. Cruden, Performance of recovered and reagent grade electrolyte in a soluble lead redox cell, J. Energy Storage (2018;20(August) 49–56, https://doi.org/10.1016/j.est.2018.08.017.
[5] A. Oury, A. Kirchev, Y. Bultel, E. Chainet, PbO2/Pb2+ cycling in methanesulfonic acid and mechanisms associated for soluble lead-acid flow battery applications,

Electrochim. Acta 71 (2012) 140–149, https://doi.org/10.1016/j.electacta.2012.03.116.
[6] M.D. Gernon, M. Wu, T. Buszta, P. Janney, Environmental benefits of methanesulfonic acid: comparative properties and advantages, Green Chem. 1 (3) (1999) 127–140, https://doi.org/10.1039/a900157c.
[7] M.G. Verde, K.J. Carroll, Z. Wang, A. Sathrum, Y.S. Meng, Achieving high efficiency and cyclability in inexpensive soluble lead flow batteries, Energy Environ. Sci. 6 (6) (2013) 1573–1581, https://doi.org/10.1039/c3ee40631h.
[8] A.A. Shah, X. Li, R.G.A. Wills, F.C. Walsh, A mathematical model for the soluble lead-acid flow battery, J. Electrochem. Soc. 157 (5) (2010) A589, https://doi.org/10.1149/1.3328520.
[9] M.N. Nandanwar, S. Kumar, Modelling of effect of non-uniform current density on the performance of soluble lead redox flow batteries, J. Electrochem. Soc. 161 (10) (2014) A1602–A1610, https://doi.org/10.1149/2.0281410jes.
[10] E.J. Fraser, Ranga Dinesh Kkj, R.G.A. Wills, A two dimensional numerical model of the membrane-divided soluble lead flow battery, Energy Rep. 7 (2021) 49–55, https://doi.org/10.1016/J.EGYR.2021.02.056.
[11] M.N. Nandanwar, K.S. Kumar, S.S. Srinivas, D.M. Dinesh, Pump-less, free-convection-driven redox flow batteries: modelling, simulation, and experimental demonstration for the soluble lead redox flow battery, J. Power Sources 454 (2020), 227918, https://doi.org/10.1016/J.JPOWSOUR.2020.227918.
[12] K.T. Cho, P. Albertus, V. Battaglia, A. Kojic, V. Srinivasan, A.Z. Weber, Optimization and analysis of high-power hydrogen/bromine-flow batteries for grid-scale energy storage, Energy Technol. 1 (10) (2013) 596–608, https://doi.org/10.1002/ente.201300108.
[13] V. Viswanathan, A. Crawford, D. Stephenson, et al., Cost and performance model for redox flow batteries, J. Power Sources 247 (2014) 1040–1051, https://doi.org/10.1016/j.jpowsour.2012.12.023.
[14] D. Reed, E. Thomsen, W. Wang, et al., Advances in PNNL ' S Mixed Acid Redox Flow Battery Stack, 2016. Published online.
[15] A. Crawford, V. Viswanathan, D. Stephenson, et al., Comparative analysis for various redox flow batteries chemistries using a cost performance model, J. Power Sources 293 (2015) 388–399, https://doi.org/10.1016/j.jpowsour.2015.05.066.
[16] S.M. Vaca, C. Patsios, P. Taylor, Enhancing frequency response of wind farms using hybrid energy storage systems, in: 2016 IEEE International Conference on Renewable Energy Research and Applications, ICRERA 2016. IEEE, 2017, pp. 325–329, https://doi.org/10.1109/ICRERA.2016.7884560.
[17] D. Roberts, S. Brown, Flow batteries for energy management: novel algebraic modelling approaches to properly assess their value, J. Energy Storage 26 (2019), https://doi.org/10.1016/j.est.2019.100977.
[18] T.A. Nguyen, M.L. Crow, A.C. Elmore, Optimal sizing of a vanadium redox battery system for microgrid systems, IEEE Trans. Sustain. Energy 6 (3) (2015) 729–737, https://doi.org/10.1109/TSTE.2015.2404780.
[19] Mobile power - energy and transport in africa. https://www.mobilepower.co/#our-batteries. (Accessed 8 September 2022). Accessed.
[20] JRC. JRC, Photovoltaic geographical information system (PVGIS) - European commission, Photovolt. Geogr. Inf. Syst. Publ. Online (2017). https://re.jrc.ec.europa.eu/pvg_tools/en/tools.html. (Accessed 8 September 2022). Accessed.
[21] P. Denholm, D.J. Arent, S.F. Baldwin, et al., The challenges of achieving a 100% renewable electricity system in the United States, Joule 5 (6) (2021) 1331–1352, https://doi.org/10.1016/j.joule.2021.03.028.
[22] K. Deb, A. Pratap, S. Agarwal, T. Meyarivan, A fast and elitist multiobjective genetic algorithm: NSGA-II, IEEE Trans. Evol. Comput. 6 (2) (2002) 182–197, https://doi.org/10.1109/4235.996017.
[23] J. Blank, K. Deb, Pymoo: multi-objective optimization in Python, IEEE Access 8 (2020) 89497–89509.
[24] E.A. Kaminski, R.F. Savinell, A technique for calculating shunt leakage and cell currents in bipolar stacks having divided or undivided cells, J. Electrochem. Soc. 130 (5) (1983) 1103–1107, https://doi.org/10.1149/1.2119891.
[25] N. Jaiswal, H. Khan, K. Ramanujam, The combined impact of trimethyloctadecylammonium chloride and sodium fluoride on cycle life and energy efficiency of soluble lead-acid flow battery, J. Energy Storage 54 (2022), 105243, https://doi.org/10.1016/j.est.2022.105243.
[26] D. Pletcher, R. Wills, A novel flow battery: a lead acid battery based on an electrolyte with soluble lead(II): Part II. Flow cell studies, Phys. Chem. Chem. Phys. 6 (8) (2004) 1779–1785, https://doi.org/10.1039/b401116c.
[27] M. Krishna, R.G.A. Wills, A.A. Shah, D. Hall, J. Collins, The separator-divided soluble lead flow battery, J. Appl. Electrochem. 48 (9) (2018) 1031–1041, https://doi.org/10.1007/S10800-018-1230-2/TABLES/6.
[28] C.P. Zhang, S.M. Sharkh, X. Li, F.C. Walsh, C.N. Zhang, J.C. Jiang, The performance of a soluble lead-acid flow battery and its comparison to a static lead-acid battery, Energy Convers. Manag. 52 (12) (2011) 3391–3398, https://doi.org/10.1016/j.enconman.2011.07.006.
[29] Finish Thompson Inc, Sealless pumps - DB3. https://www.finishthompson.com/pumps/sealless-pumps/db-series-plastic-mag-drive-pumps/db3/. (Accessed 6 December 2022). Accessed.
[30] K. Muthu, Improvements to the Soluble Lead Redox Flow Battery, 2017, https://doi.org/10.1016/0041-2678(70)90288-5. Published online.
[31] B. Koo, D. Lee, J. Yi, et al., Modeling the performance of a zinc/bromine flow battery, Energies 12 (6) (2019) 1–13, https://doi.org/10.3390/en12061159.
[32] HOP MP-40RX 85LPM 220v, https://www.alibaba.com/product-detail/HOP-MP-40RX-85LPM-220v-Homebrew_1600225519176.html?spm=a2700.galleryofferlist.normal_offer.d_title.5a787b25PyUf2n. (Accessed 16 December 2022).
[33] BASF invests in capacity expansion for methane sulfonic acid. https://www.basf.com/global/en/media/news-releases/2020/01/p-20-115.html. (Accessed 2 February 2022). Accessed.
[34] S. Kappenthuler, S. Olveira, J. Wehrli, S. Seeger, Environmental assessment of alternative methanesulfonic acid production using direct activation of methane, J. Clean. Prod. 202 (2018) 1179–1191, https://doi.org/10.1016/j.jclepro.2018.07.284.
[35] S. Ha, K.G. Gallagher, Estimating the system price of redox flow batteries for grid storage, J. Power Sources 296 (2015) 122–132, https://doi.org/10.1016/j.jpowsour.2015.07.004.
[36] Fraunhofer Umsicht, Volterion and Fraunhofer UMSICHT: step towards mass market for redox flow batteries – startup|Energy. https://startup-energy.org/volterion-and-fraunhofer-umsicht-step-towards-mass-market-for-redox-flow-batteries/?lang=en. (Accessed 3 August 2022).
[37] J. Collins, X. Li, D. Pletcher, et al., A novel flow battery: a lead acid battery based on an electrolyte with soluble lead(II). Part IX: electrode and electrolyte conditioning with hydrogen peroxide, J. Power Sources 195 (9) (2010) 2975–2978, https://doi.org/10.1016/j.jpowsour.2009.10.109.
[38] E. Rackley, A. Wade, E. Santos, C. Kohler, J. Lindsay, R. Pell, SIZE MATTERS : THE ECONOMIC AND ENVIRONMENTAL IMPACT OF SMALLER EV BATTERIES, 2022; (June. https://uploads-ssl.webflow.com/6008a2327223f98143f46e18/62e265d249364e247acd1242_Half-Size Battery LCA.pdf.
[39] X. Yan, A submillimeter bundled microtubular flow battery cell with ultrahigh volumetric power density, Photovolt. Geogr. Inf. Syst. Publ. Online (2017), https://doi.org/10.1073/pnas, 2017.